Mohedano, M.; Blawert, C.; Zheludkevich, M.L.:

Cerium-based sealing of PEO coated AM50 magnesium alloy

In: Surface and Coatings Technology (2015) Elsevier

DOI: 10.1016/j.surfcoat.2015.01.003

Cerium-based sealing of PEO coated AM50 magnesium alloy

M. Mohedano*, C. Blawert, M.L. Zheludkevich

Helmholtz Zentrum Geesthacht, Magnesium Innovation Centre, Institute of Materials Research, Max-Planck-Str. 1, D-21502 Geesthacht, Germany.

*Corresponding author. Tel:+494152871956; Fax:+494152871960

E-mail: marta.mohedano@hzg.de

Abstract

Environmentally friendly Ce-based sealing post-treatments were developed for PEO coatings on AM50 magnesium alloy. The influence of the $Ce(NO_3)_3$ concentration in the Ce bath and the time of the sealing process were evaluated in terms of morphological and structural properties using SEM, EDS and XRD. Ce content in the layer increased with both the amount of salt in the solution and the time of the sealing post-treatment process due to a higher Ce products accumulation into the pores and cracks of the coatings. Sealed PEO coatings revealed an improvement in the corrosion protection properties as measured by electrochemical impedance spectroscopy. Differences in the corrosion resistance values for the sealed coatings indicate a strong relation between the parameters of the sealing process and its effectiveness, showing higher resistance for the sealed PEO coating developed after 3 h of immersion in 10 g/l $Ce(NO_3)_3$ sealing bath.

Keywords: Magnesium; PEO; Cerium; Sealing; Corrosion.

1. Introduction

The growing demand for lightweight materials in the automotive, aeronautic and recreational industries has triggered renewed attention for magnesium alloys owing to their outstanding specific strength, high damping capacity, good castability, machinability and weldability [1,2]. However, high chemical reactivity and poor corrosion and wear resistance limit the widespread use of magnesium alloys in many applications [3-5].

The addition of several alloying elements such as aluminium, zinc and rare earths have been reported to improve the corrosion resistance of Mg alloys [6,7]. However, the technological requirements for several applications remains still unsatisfied [8].One of the effective ways to improve the corrosion resistance of Mg-based substrates is application of protective coatings, which provide a barrier against aggressive species and reduce detrimental effects from the environment [9]. There are several technologies available for coating magnesium alloys. These mainly include electrochemical plating, conversion coatings, anodizing, hybrid sol-gel coatings, gas-phase deposition processes, laser surface melting and organic/polymer coatings [10-14]. Among these coating processes, plasma electrolytic oxidation (PEO) is a promising surface treatment technique to build ceramic-like layers on Mg, Al, Ti and other valve metals. This technique involves polarization of the valve material under high voltages in an appropriate electrolyte, with the generation of a large number of short-lived microdischarges caused by dielectric breakdown and the formation of plasma modifying the coating with the incorporation of species from the electrolyte [15-18]. The main advantages of PEO coatings include improved corrosion and wear resistance, high dielectric strength, heat resistance and suitable surface morphology for topcoat paints and other metals/ceramics to create duplex coatings [19,20].

In the particular case of Mg and its alloys, some commercial PEO processes are already available [21-23]. However these treatments often contain non-environmentally friendly

components, like chromic acid and fluoride based compounds, therefore some effort has been made to solve this disadvantage by using electrolytes based on silicates and phosphates [24-26]. Coatings can be formed under DC, AC or bipolar electrical regimes and the appropriate adjustment of the electrical parameters reduce the porosity of the coating and increase the inner dense layer thickness [27,28]. However, the presence of the pores is unavoidable in the PEO coatings leading to decrease in barrier properties. The pores compromise the corrosion resistance of such coatings, particularly in presence of Cl^- ions, and this may restrict any future potential application of PEO on Mg alloys.

Different surface post-treatment approaches for PEO coatings were suggested including organic, sol-gel and polymer coatings in order to avoid the early failure of PEO coatings on Mg alloys due to their permeability to the environment [29-31]. Among these, the Ce-based post-sealing treatments for PEO on Mg can be considered as one of the most promising candidates in terms of costs, efficiency and environmental compatibility [32,33].

The effectiveness of cerium-based coatings has been widely demonstrated for aluminium alloys in terms of corrosion protection performance [34-36]. Over the last years promising results have been also reported for magnesium and its alloys [37-40]. However the suitability of Ce-based post-treatments for PEO coatings is not clear due to the complex composition and morphology of these coatings and only there are few investigations to date. Lim *et al.* conducted investigations with DC PEO coated AZ31 and found a slight improvement in the corrosion resistance after post-sealing based on $CeCl_3$ solution [41]. Laleh *et al.* also achieved better corrosion resistance for a short-term exposure in chloride media (30 min) after the application of sealing based on $CeCl_3$ on DC PEO coated AZ91 [42].

However to date there is no sealing method based on cerium aqueous solutions able to improve the corrosion properties of PEO coatings on magnesium significantly. Moreover, no systematic study was performed and some very important aspects remain somewhat unclear

with respect to: i) distribution of the Ce-containing compounds through the coating, particularly for PEO coatings developed under AC electrical regimes ii) corrosion resistance for longer times of immersion iii) effect of sealing process parameters on the performance of coatings.

The main goal of present work is to develop a Ce-based sealing post-treatment for environmentally friendly PEO coatings deposited on AM50 magnesium alloy. The systematic study on the influence of the duration of post-treatment and the bath composition on the corrosion protection performance is conducted with a set of complementary electrochemical, structural and microscopic methods.

2. Material and methods

2.1. Materials

AM50 magnesium alloy (mass fraction: 4.4-5.5% Al, 0.26-0.6% Mn, max 0.22% Zn, max 0.1% Si, and Mg balance) of size 15 mm × 15 mm × 4 mm was used as the substrate for PEO coating process.

Specimens were ground successively with emery papers of 500, 800 and 1200 grit size and cleaned with ethanol prior to PEO treatment.

2.2. PEO treatments

AC PEO treatments were conducted for 600 s using a PE Pulse Reverse Power Supply rated at max. 500V/24A mode pulses in alkaline silicate solution (10 g/l Na_2SiO_3 + 2 g/l KOH) at constant voltage. A square waveform voltage signal was applied at 500 Hz frequency with a positive-to-negative pulse ratio of 420/-60 V. An initial ramp of 60 s was used to achieve the

voltage amplitude. The PEO treatments were performed at 10 °C ± 2 °C. After PEO, the specimens were rinsed in distilled water and dried in warm air.

2.3. Sealing post-treatments

Three different post-treatments based on $Ce(NO_3)_3$ were performed by immersing the PEO coated specimens under the conditions described in Table 1. After that, sealed samples were rinsed with ethanol and dried in warm air.

2.4. Characterization

Plan views and cross-sections of coatings were examined with a Tescan Vega3 SB scanning electron microscope (SEM) equipped with energy dispersive X-ray (EDX) spectrometer. Cross-sections were prepared by grinding through successive grades of silicon carbide paper, with final polishing to a 1 μm diamond finish. Phase composition was examined by X-ray diffraction (XRD), with a Bruker X-ray diffractometer with Cu Kα radiation (Cu Kα = 1.54056 Å) at a scanning speed of 0.01 s^{-1} in 2θ scan range of 2θ from 10 to 90°.

2.5. Electrochemical tests

Electrochemical tests were conducted in a stirred aqueous 0.5 wt.% NaCl solution at 22 ± 0.5 °C using a Gill AC computer-controlled potentiostat. All potentials were measured with respect to Ag/AgCl reference electrode. A platinum mesh was used as the counter electrode. Electrochemical impedance spectroscopy (EIS) measurements were performed at different times up to 3 days applying a sinusoidal perturbation of 10 mV RMS amplitude and a

frequency sweep from 0.01 Hz to 30 kHz. All measurements were repeated twice with good reproducibility, using a working electrode area of 0.5 cm^2.

The impedance spectra were analyzed with ZView software, the goodness of fit of the simulated spectra corresponded to chi-squared (square of the standard deviation between the original data and the calculated spectrum) values <0.01. The errors for the individual parameters of the equivalent electrical circuits (such as CPE and R) were <5%.

3. Results and discussion

3.1. Coating morphology and microstructure

The optical micrographs of unsealed and sealed coatings are shown in Fig. 1. PEO coating based on a silicate electrolyte revealed a white gray color typical for this type of coatings [15,43] (Fig. 1 (a)). Sealing post-treatments changed the color of the coated specimens into pale yellow (Fig. 1 (b)) and dark yellow (Fig. 1 (c,d)) depending on the treatment conditions due to the presence of Ce-containing products [44]. Compared with the time needed for traditional cerium-based conversion treatments, the post-treatments developed in this work showed deposition of Ce-species after 20 min of immersion [45,46]. This may be due to the presence of hydrogen peroxide in the sealing bath that has been reported to increase the kinetics of the conversion process oxidizing Ce (III) into Ce (IV) and leading to a higher deposition rate for Ce-species [47,48].

The sealing of the pores is clearly evidenced by SEM/EDS analysis of the surface. Fig. 2 shows the surface micrographs of AM50 alloy after the different surface treatments. Unsealed PEO coating (Fig. 2 (a)) exhibited a typical crater-like porous morphology with a pore size between 0.4μm-15μm. The pores arise at the sites of the discharges channels due to the gas evolution through the molten oxide material during the PEO process [49]. The number of

open pores decreases for all the coatings after the sealing post-treatments due to the accumulation of Ce-containing products in the pores. The sealing effectiveness increase with the amount of $Ce(NO_3)_3$ in the solution and with the time of the post-treatment process (Fig. 2 (b-d)). In particular for PEO_SCe_10g_3h most of the pores disappeared and the surface was almost fully sealed after 3 h of treatment (Fig. 2 (d)).

The higher magnification images of the sealed PEO coatings and the respective EDS mapping analysis of the Ce element revealed morphological and microstructural differences of the surfaces (Fig. 3). In case of PEO_SCe_3g_20min, larger pores were partially filled with Ce-containing products and the average Ce concentration determined by EDS on a large area was 0.3 at.% (Fig. 3 (a,b)). An increase in the concentration of Ce salt in the sealing solution (up to 10 g/l), leads to a higher accumulation of Ce products into the pores and cracks of the coatings resulting in an increase of Ce concentration to 0.8 at.% (Fig. 3 (c,d)). The most significant differences were observed for the PEO_SCe_10g_3h specimen, where a Ce-rich layer covers the surface and large deposits of Ce-containing products are located in the initial crater-like pores (Fig. 3 (e,f)). Some cracks are observed on the Ce-rich layer and this is likely to be related to the dehydration of the surface after the treatment [50]. Sealed PEO coating developed under these conditions, showed the highest average Ce concentration (2.5 at.%) determined by EDS.

Fig. 4 shows the cross sections of the coatings along with the X-ray elemental mapping of Si (for PEO) and Ce (for sealed PEO). PEO coating shows a non uniform thickness and grow into the substrate and outwards to the coating surface simultaneously [51], to a maximum of 30-40 μm (Fig. 4 (a)). The coating consists of a three-layered structure with a denser Si-rich outer part (less than 40% of the coating thickness with through-going discharge channels), followed by a very porous section (about 59% of the coating thickness) and an inner and

denser layer (about 1% of the coating thickness) mainly composed of Mg and O with traces of Si (Fig. 4 (b)).

In case of sealed coatings, X-ray elemental mapping confirms the presence of cerium and demonstrates the significant influence of the deposition parameters: i) the concentration of Ce salt in the sealing solution (3 g/l and 10 g/l) and ii) the time of the post-sealing treatment (20 min and 3 hours). PEO_SCe_3g_20min backscattered image shows a slight decrease of the coating thickness which indicates a slight dissolution of the coating during the post-treatment. Only a minor concentration of Ce was found on the top of the outer layer from EDS mapping (Fig. 4 (c,d)). An increase in the Ce salt content in the sealing solution up to 10 g/l favored the deposition of Ce-rich products through the internal cracks, penetrating approx. 40% into the thickness of the PEO layer. Moreover, an important reduction of the PEO coating thickness up to approx. 10 μm in some areas was observed and is related to a higher dissolution of the oxide layer compared to PEO_SCe_3g_20min specimen (Fig. 4 (e,f)). The cross-section for PEO_SCe_10g_3h (Fig. 4 (g,h)) reveals the highest reduction of the thickness of the coating to approx. 15 μm in some areas and according to this, also the highest Ce- precipitation on the surface of the remaining PEO coating. Ce-containing products penetrated approx. 100% into the thickness of the PEO coating blocking its internal porosity and cracks.

The microstructural characterization of PEO coatings after all the different sealing post-treatments revealed no evidence of Ce-containing products proceeding from the reaction with the matrix. This suggests that the Ce deposition does not follow the general mechanism of cerium conversion treatments based on an increase in solution pH at the cathode interface, due to the polarization of the substrate, and the precipitation of cerium compounds in those areas [52]. In the sealed coatings developed in this work the barrier inner layer, which is the major contributor to corrosion protection [53], remains intact. Therefore, for this type of PEO coatings, the formation of Ce-rich products is associated only with the chemical dissolution of

the coating and peroxide triggered processes. The process can be summarized as: i) chemical dissolution of $MgO/MgSiO_4$ in acidic solutions locally increases the pH values [54,55] ii) high local pH values facilitates the precipitation of insoluble oxide/hydroxide Ce compounds [56].

These results provide new information about the mechanism of rare earth sealing process of porous PEO coatings for Mg alloys that had remained unclear. Previous studies reported some differences in the outcomes: Lim *et al.* conducted investigations with DC pulse PEO coating on AZ31 alloy after $CeCl_3$ based sealing and found that Ce-containing precipitates observed in the coating were initially formed at the interface between PEO coating and the substrate [41]. Laleh *et al.* also reported the presence of Ce species on the surface of DC PEO coating on AZ91 alloy after $CeCl_3$ based sealing, but in this case there was no evidence where the chemical reaction/conversion process took place [42].

This information indicates that there are two factors that might influence the sealing mechanism of PEO: i) the presence of Cl^- ions in the sealing solution might lead to a higher degradation of the coating favoring its penetration across the porous and cracks and reaction with the metal surface [57] ii) the application of AC regimes for PEO treatments that achieve a higher resistance in the inner layer [58], might have the opposite effect preventing the penetration of the sealing solution through this inner layer and therefore the contact with the alloy.

X-ray diffraction (XRD) analysis indicated that the PEO coating produced in silicate electrolyte is composed predominantly of two crystalline phases: Mg_2SiO_4 and MgO (Fig. 5). The coating layer on sample treated for 20 min using 3 g/l $Ce(NO_3)_3$, mainly showed strong diffraction peaks of the PEO coating. It is probable that the Ce-containing products layer is either too thin or incomplete as the treatment is not sufficient for the formation of a homogeneous coating as was observed with the SEM.

The XRD patterns from the sealed PEO coatings developed using 10 g/l $Ce(NO_3)_3$, revealed the formation of CeO_2 and Ce_2O_3 with stronger intensity peaks for longer sealing post-treatment process (PEO_SCe_10g_3h). Similar compositions have been reported for Ce conversion treatments developed on magnesium and its alloys [50,38]. The presence of CeO_2 and Ce_2O_3 was also found in Ce-based conversion treatments using $CeCl_3$ bath on AZ31 coated by PEO [41]. The Ce^{3+} (hydroxide/oxide) species in contact with O_2 can be partially oxidized to Ce^{4+} (hydroxide/oxide). According to Wu *et al*. the Ce-containing products inside the cracks and porous of PEO coatings are composed of Ce^{3+} species and the external film of mixture of Ce^{3+} and Ce^{4+} species [59]. It is also possible that amorphous Ce conversion products are present after the sealing process, as reported previously for similar treatments [60].

3.2 Electrochemical impedance spectroscopy results

Electrochemical impedance spectroscopy is a powerful tool which allows correlation of electrical characteristics of the coated metallic substrate with corrosion resistance of the system. The frequency dependence of the complex impedance of the coated substrate permits effective evaluation of the different components of the coated system such as capacitance and resistance of the protective layers, polarization resistance and double layer capacitance associated with electrochemical activities on the surface. EIS method is used in the present work to gain a better understanding of the mechanism of the PEO coatings degradation and the effect of the Ce-based sealing post-treatments on the anti-corrosion performance [61,62].

Bode (a,b) and Nyquist (c) diagrams of EIS response in 0.5 wt.% NaCl solution measured up to 3 days of immersion are shown in: Fig. 6 for PEO, Fig. 7 for PEO_SCe_3g_20min, Fig. 8 for PEO_SCe_10g_20min and Fig. 9 for PEO_SCe_10g_3h.

The equivalent circuit used for simulation of the electrical parameters is shown in Fig. 10 inserted in the example of the fitting of the experimental data. Constant Phase Elements (CPE) were used instead of capacitances in order to account for non-ideal behavior of the system. Good fits of the experimental data, with chi-squared values in the range of 0.001–0.0001, were obtained using a cascade equivalent electrical circuit where CPE_{out} and R_{out} correspond to the capacitive and resistive behavior of the combination of outer and intermediate porous layers of the PEO coatings. This combined response is associated with the porosity interconnecting these two layers and for further analysis of the impedance spectra, PEO coatings are considered to have a two-layered structure: i) an outer layer (combination of outer and intermediate) characterized for through-going discharge channels and porosity and ii) a denser inner barrier part. CPE_{in} and R_{in} are associated with the capacitive and resistive performance of the barrier inner part of the PEO coating respectively. The corrosion processes can be described by the double layer capacitance on the electrolyte/metal interface (CPE_{dl}) and the polarization resistance (R_{polar}), which is the Faradaic charge transfer resistance related to electrochemical reactions in the same electrolyte/metal interface region [63].

The impedance of a CPE is calculated as $Z = 1/[CPE\ (j\omega)n]$; where ω i s radial frequency, n is the exponential factor ($-1 \leq n \leq 1$) and $j = \sqrt{-1}$ is the imaginary number. CPE corresponds to a numerical value of admittance of the system, 1/Z, at $\omega = 1$ rad s^{-1}. With n = 1, constant phase element becomes an ideal capacitor. For all the equivalent circuits R_s corresponds to the solution resistance.

Based on this equivalent circuit, three time constants corresponding to three relaxation processes are found in the response of the coated materials. However, the visibility of these

time constants in the impedance spectra is not possible for all the times due to strong overlapping.

Up to 1 day of immersion, the impedance response for unsealed PEO (Fig. 6) shows the presence of different relaxation processes. The outer porous layer of the coating is responsible for the high-frequency relaxation process (10^3 Hz), whereas the middle frequency response of the system (10^1-10^2 Hz) can be attributed to the inner barrier layer of the PEO coating. In fact these two components are hard to distinguish in the beginning because of the strong overlapping. The separation becomes obvious after a longer immersion period. The low frequency time constant (0.1 Hz) observed since the beginning can be ascribed to the starting electrochemical activities on the alloy surface. These corrosion processes can be described by the double layer capacitance on the electrolyte/metal interface and the polarization resistance.

After 1 day of immersion, the time constant at high frequencies corresponding to the outer porous layer of the PEO coating has almost disappeared. This indicates that the electrolyte can easily penetrate through the outer part and a chemical degradation of the coating occurs to a certain degree leading to the loss of the barrier properties of outer layer. The time constant at middle frequencies (10^2 Hz) becomes better visible now. The inner barrier layer dominates the response of the system in this situation.

For sealed PEO coatings (Fig. 7-9), the impedance spectra show similar features as for the unsealed PEO coating. After one day of immersion in 0.5 wt.% NaCl solution, the resistance of the outer layer of the PEO coating is unappreciable and the time constant at lower frequencies can be associated with the corrosion process. The model of the equivalent circuit for unsealed PEO also describes the spectra for sealed PEO (Fig. 10). However, the obtained values of calculated parameters demonstrate that the physical properties of structural elements differ due to the presence of Ce-containing products, showing better corrosion properties. This improvement of the corrosion behavior, has been also reported for Ce conversion

coatings on aluminium [59] zinc [64] and magnesium alloys [65]. In particular, Wu *et al.* [59] suggested that the impedance spectrum after Ce conversion process was influenced by the Ce-rich products precipitated on the materials leading to a capacitive and resistive behavior of Ce-rich coating. For sealed PEO coatings, the most important effect seems to be the stabilization of the inner layer during longer immersion tests. The time constant responsible for this component is much better defined, demonstrating higher values of inner layer resistance. The stabilization of the inner layer increase with the amount of $Ce(NO_3)_3$ in the solution and with the time of the post-treatment process.

In order to evaluate the degradation behavior of unsealed and sealed PEO coatings and the influence of the different sealing parameters, the values of the total resistance ($R_{total(out+in+polar)}$) with the time of immersion in 0.5 wt.% NaCl solution are shown in Fig. 11.

In addition, for a better understanding of the corrosion mechanism, the evolution of the polarization (Fig. 12 (a)) and inner resistance (Fig. 12 (b)) with the immersion time are shown separately. These resistance values were obtained by fitting the equivalent circuit to the impedance data and are presented with respecting their fitting errors. Low values of the outer resistance ($R_{out} < 10^3\ \Omega\ cm^2$) and their fast decrease in the first 10 h indicate that the outer layer is not an important contributor to the corrosion protection and therefore not important for the analysis of the corrosion mechanism for this type of coatings [66].

For immersion times up to 3 h, no significant differences in the values of R_{total} are observed for the coated materials due to the good protective character of PEO layer at this stage (Fig. 11). For longer immersion times, unsealed PEO coating reveals the typical behavior for this type of coatings with a continuous decrease of R_{total} up to 2 orders of magnitude. A different response depending on the parameters of the sealing process is observed for the sealed PEO coatings. A continuous decrease in the R_{total} for PEO_SCe_3g_20min up to one order of magnitude indicates also a gradual corrosion process, showing the same tendency as the

unsealed coating. More effective sealing post-treatments processes were found for PEO coatings sealed in a solution containing 10 g/l $Ce(NO_3)_3$ (after 20 min and 3 h of post-treatment). They show an increase in the R_{total} values during the early stages (up to 24 h) followed by a decrease associated with corrosion processes, which is more significant for PEO_SCe_10g_20 min. This tendency is due to the evolution of the R_{polar} and related to the formation of corrosion products with some protective character (Fig. 12 (a)).

After 3 days of immersion (Fig. 11) all the coated materials show a degradation process characterized by a decrease of the total resistance, but also a clear beneficial effect of the Ce-based sealing post-treatments was observed. Unsealed PEO coating reveals the lowest value after 3 days of immersion (20 $k\Omega\ cm^2$) due to its higher susceptibility to corrosion. Differences in the resistance values for the sealed coatings, up to one order the magnitude, indicate a strong relation between the parameters of the sealing process and its effectiveness. According to the total resistance values, (PEO_SCe_10g_3h > PEO_SCe_10g_20min > PEO_SCe_3g_20min > PEO), higher concentrations of cerium salt in the bath (10 g/l of $Ce(NO_3)_3$) and longer times of sealing process (3 h) lead to a better corrosion properties of the sealed coatings. This is in agreement with the morphology and microstructure examination of the coatings, which show for those conditions a higher accumulation of Ce products blocking the pores and the internal cracks.

In addition, the analysis of the R_{in} with time of immersion in 0.5 wt.% NaCl solution (Fig. 12 (b)) shows a stabilization of the inner layer for the Ce containing coatings. R_{in} results obtained for shorter times of immersion (up to 10 h) show slightly higher values of sealed coatings compared with the unsealed PEO coating. For longer immersion times (up to 3 days) a different response is revealed showing different effects: i) a long-term protection effect of the post-treatments: an increase of the R_{in} is observed for all the sealed coatings compared with the unsealed PEO coating ii) an influence of the Ce sealing parameters: higher values

were obtained by increasing both the amount of $Ce(NO_3)_3$ in the solution and the post-treatment process time and iii) a stabilization of the inner layer: sealed PEO coatings developed using 10 g/l $Ce(NO_3)_3$ show an increase of the R_{in} values after 10 h of immersion that might be related to the formation of corrosion products containing Ce which act as a temporary protective layer together with the original inner layer. In particular for PEO_SCe_10g_3h this effect is more significant, revealing an increase in R_{in} after 3 days of immersion to $10^5\ \Omega\ cm^2$.

The better corrosion properties of the sealed PEO coatings might be related to a combination of different effects: i) microstructural effect: sealed coatings show that the large-sized pores and through-going paths across the whole layer were partially filled with Ce-containing products and that obstruct the permeation of the electrolyte into the inner coating ii) Ce-rich corrosion products accumulation effect: the chemical degradation of the coating leads to the migration of Ce-containing products from the PEO surface across the porosity of the coating improving the protective ability of the inner layer. These hypothesis are in accordance with the analysis of the cross-section of EIS tested coated materials after immersion in naturally-aerated 0.5 wt.% NaCl solution for 3 days (Fig. 13). No sign of severe corrosion attack was observed in the coating/substrate interface and a significant accumulation of products mainly consisted of Ce-rich corrosion products were found in the porosity close to the inner layer of the coating. In addition, there might be an active effect of Ce ions in the coatings: when the electrolyte penetrates the PEO coating, some of the Ce containing products might convert into the Ce^{3+} ions. At the same time, a nano-scale corrosion process might occur in the inner layer leading to an increase in the pH, inducing Ce^{3+} deposition that can stabilizes the inner layer. The active corrosion protection or “self-healing” is generally defined as the recovery of coating integrity after some damage, and Ce-containing coatings were found to confer active protection for aluminium alloys coated by sol-gel, epoxy or chitosan layer [67-69]. According

to this active corrosion protection effect, it has been also report that cerium cations may react with silicates leading to the formation of a protective "self-healing" film [70]. In particular, for silicate based PEO coatings and for prospect work, it would be interesting to analyze these coatings with high resolution microscopy in order to observe structural modifications to the inner layer.

4. Conclusions

Environmentally friendly Ce-based post-sealing treatments were successfully developed on PEO coated AM50 magnesium alloy. Microstructural characterization showed that the Ce content of the coatings increased with both the amount of $Ce(NO_3)_3$ in the solution and the sealing post-treatment process time, leading to a higher accumulation of Ce products into the porous and cracks in the coatings. The formation of Ce-containing products is associated only with the chemical dissolution of the coating and there was no evidence of Ce-containing products proceeding from the reaction with the matrix. XRD patterns showed the formation of CeO_2 and Ce_2O_3 for sealed PEO coatings developed using 10 g/l of $Ce(NO_3)_3$.

Electrochemical impedance response revealed that the corrosion properties of the coatings improved after the application of the sealing post-treatments. Differences in the resistance values for the sealed coatings indicate a strong relation between the parameters of the sealing process and its effectiveness: higher concentrations of cerium salt in the bath (10 g/l of $Ce(NO_3)_3$) and longer times of sealing process (3 h) lead to a better corrosion properties. The sealed PEO coating developed after 3h of immersion in 10 g/l $Ce(NO_3)_3$ solution showed the highest R_{in}, R_{polar} and therefore the highest total impedance after 3 days of immersion in 0.5 wt.% NaCl. Better corrosion properties of the sealed coatings are due to a partial blocking of the internal porosity of the coatings and the stabilization of the inner layer during longer immersion tests.

Acknowledgements

M. Mohedano is grateful to the Alexander von Humboldt Foundation, Germany, for the award of AvH research fellowship. The technical support from Mr. U. Burmester and Mr. V. Heitmann during the course of this work is gratefully acknowledged.

References

[1] B.L. Mordike, T. Ebert, Magnesium Properties - applications – potential, Mat. Sci. Eng. A. 302 (2001) 37-45.

[2] M.K. Kulekci, Magnesium and its alloys applications in automotive industry, Int. J. Adv. Manuf. Technol. 39 (2008) 851-865.

[3] R. Ambat, N.N. Aung, W. Zhou, Studies on the influence of chloride ion and pH on the corrosion and electrochemical behaviour of AZ91D magnesium alloy, J. Appl. Electrochem. 30 (2000) 865-874.

[4] K.U. Kainer, P. Bala Srinivasan, C. Blawert, W. Dietzel, 3.09-Corrosion of magnesium and its alloys. In: Cottis B., Graham M., Lindsay R., Lyon S., Richardson T., Scantlebury D., Stott H., editors. Shreir's Corrosion. Elsevier; Oxford, UK: 2010. pp. 2011–2041.

[5] M. Mohedano, A. Pardo, M.C. Merino, K. Paucar, P. Casajús, E. Matykina, Salt spray corrosion behaviour of new Mg-Al alloys containing Nd or Gd, Corros. Eng. Sci. Technol. 48 (2013) 183-193.

[6] E. Ghali, W. Dietzel, K.U. Kainer, General and Localized Corrosion of Magnesium Alloys, Mater. Eng. Perform. 131 (2004) 7-23.

[7] G.L. Song, A. Atrens, Corrosion mechanisms of magnesium alloys, Adv. Eng. Mater. 1 (1999) 11-33.

[8] E. Aghion, B. Bronfin, Magnesium alloys development towards the century 21st, Mater.Sci.Forum 350 (2000) 19-30.

[9] W.U. Chao-Yun, Z. Jin, State-of-art on corrosion and protection of magnesium alloys based on patent literatures, Trans. Nonferrous Met. Soc. China 21 (2001) 892-902.

[10] J.E. Gray, B. Luan, Protective coatings on magnesium and its alloys – a critical review, J. Alloys Compd. 336 (2002) 88-113.

[11] K.T. Rie, J. Whole, Plasma – CVD of TiCN and ZrCN films on light metals, Surf. Coat. Technol. 112 (1999) 226-229.

[12] G.L. Song, Electroless deposition of a pre-film of electrophoresis coating and its corrosion resistance on a Mg alloy, Electrochim. Acta 55 (2010) 2258-2268.

[13] R.G. Hu, S. Zhang, J.F. Bu, C.J. Lin, G.L. Song, Recent progress in corrosion protection of magnesium alloys by organic coatings, 73 (2012) 129-141.

[14] M. Qian, D. Li, S.B. Liu, S.L. Gong, Corrosion performance of laser-remelted Al–Si coating on magnesium alloy AZ91D, Corros. Sci. 52 (2010) 3554-3560.

[15] R. Arrabal, E. Matykina, T. Hashimoto, P. Skeldon, G.E. Thompson, Characterization of AC PEO coatings on magnesium alloys, Surf. Coat. Technol. 203 (2009) 2207-2220.

[16] A.L. Yerokhin, X. Nie, A. Leyland, A. Matthews, Characterisation of oxide films produced by plasma electrolytic oxidation of a Ti–6Al–4V alloy, Surf. Coat. Technol. 130 (2000) 195-206.

[17] E. Matykina, R. Arrabal, P. Skeldon, G.E. Thompson, Investigation of the growth processes of coatings formed by AC plasma electrolytic oxidation of aluminium, Electrochim. Acta. 54 (2009) 6767-6778.

[18] C. Blawert, S. Prasad, J. Liang, Y. Huang, D. Höche, Role of sintering and clay particle additions on coating formation during PEO processing of AM50 magnesium alloy, Surf. Coat. Technol. 213 (2012) 48-58.

[19] R. Arrabal, J.M. Mota, A. Criado, A. Pardo, M. Mohedano, E. Matykina, Assessment of duplex coating combining plasma electrolytic oxidation and polymer layer on AZ31 magnesium alloy, Surf. Coat. Technol. 206 (2012) 4692-4703.

[20] G. Rapheal, S. Kumar, C. Blawert, Narendra B. Dahotre, Wear behaviour of plasma electrolytic oxidation (PEO) and hybrid coatings of PEO and laser on MRI 230D magnesium alloy, Wear 271 (2011) 1987-1997.

[21] A. S. Shatrov, V.L. Samsonov, US Patent 6896785 B2, 2005.

[22] D. Bartak, B. Lemieux, E. Woolsey, US Patent 547664, 1995.

[23] E. Schmeling, US Patent 4978432, 1990.

[24] C. Blawert, V. Heitmann, W. Dietzel, H.M. Nykyforchyn, M.D. Klapkiv, Influence of electrolyte on corrosion properties of plasma electrolytic conversion coated magnesium alloys, Surf. Coat. Technol. 201(2007) 8709-8714.

[25] R. Arrabal,A. Pardo, M.C. Merino, M. Mohedano, P. Casajús, E. Matykina, P. Skeldon,G.E. Thompson, Corrosion behaviour of a magnesium matrix composite with a silicate plasma electrolytic oxidation coating, Corros. Sci. 52 (2010) 3738-3749.

[26] C. Blawert, W. Dietzel, E. Ghali, G. Song, Anodizing treatments for magnesium alloys and their effect on corrosion resistance in various environments, Adv. Eng. Mater. 8 (2006) 511-533.

[27] R.O. Hussein, D.O. Northwood, X. Nie, The influence of pulse timing and current mode on the microstructure and corrosion behaviour of a plasma electrolytic oxidation (PEO) coated AM60B, J. Alloys Compd. 541 (2012) 41-48.

[28] S.V. Gnedenkov, O.A. Khrisanfova, A.G. Zavidnaya, S.L. Sinebryukhov, V.S. Egorkin, M.V. Nistratova, A. Yerokhin, A. Matthews, PEO coatings obtained on an Mg-Mn type alloy under unipolar and bipolar modes in silicate-containing electrolytes, Surf. Coat. Technol. 204 (2010) 2316–2322.

[29] U. Malayoglu, K.C. Tekin, S. Shrestha, Influence of post-treatment on the corrosion resistance of PEO coated AM50B and AM60B Mg alloys, Surf. Coat. Technol. 205 (2010) 1793-1798.

[30] D.K. Ivanou, M. Starykevich, A.D. Lisenkov, M.L. Zheludkevich, H.B. Xue, S.V. Lamaka, M.G.S. Ferreira, Plasma anodized ZE41 magnesium alloy sealed with hybrid epoxy-silane coating, Corros. Sci. 73 (2013) 300-308.

[31] Z. Li, X. Jing, Y. Yuan, M. Zhang, Composite coatings on a Mg–Li alloy prepared by combined plasma electrolytic oxidation and sol–gel techniques, Corros. Sci. 63 (2012) 358-366.

[32] S. Ono, K. Asami, N. Masuko, Mechanism of chemical conversion coating film growth on magnesium and magnesium alloys, Mater. Trans. 42 (2001) 1225-1231.

[33] A.K. Sharma, Chromate conversion coatings for magnesium-lithium alloys, Metal Finishing, 87 (1989) 73-74.

[34] A. Pardo, M.C. Merino, R. Arrabal, S. Merino, F. Viejo, M. Carboneras, Effect of Ce surface treatments on corrosion resistance of A3xx.x/SiCp composites in salt fog, Surf. Coat. Technol. 200 (2006) 2938-2947.

[35] D. Zhao, J. Sun, L. Zhang, Y. Tan, J. Li, Corrosion behaviour of rare earth cerium based conversion coating on aluminum alloy, J. Rare Earth 28 (2010) 371-374.

[36] A. Conde, M.A. Arenas, A. de Frutos, J. de Damborenea, Effective corrosion protection of 8090 alloy by cerium conversion coatings, Electrochim. Acta 53 (2008) 7760-7768.

[37] K. Brunelli, M. Dabala, I. Calliari, M. Magrini, Effect of HCl pre-treatment on corrosion resistance of cerium-based conversion coatings on magnesium and magnesium alloys, Corros. Sci. 47 (2005) 989-1000.

[38] L. Li, J. Lei, S. Yu, Y. Tian, Q. Jiang, F. Pan, Formation and characterization of cerium conversion coatings on magnesium alloy, J. Rare Earth, 26 (2008) 383-387.

[39] A.L. Rudd, C.B. Breslin, F. Mansfeld, The corrosion protection afforded by rare earth conversion coatings applied to magnesium, Corros. Sci. 42 (2000) 275-288.

[40] M. Dabala, K. Brunelly, E. Napolitani, M. Magrini, Cerium-based chemical conversion coating on AZ63 magnesium alloy, Surf. Coat. Technol. 172 (2003) 227-232.

[41] T.S. Lim, H.S. Ryu, S. Hong, Plasma electrolytic oxidation/cerium conversion composite coatings for the improved corrosion protection of AZ31 Mg alloys, J. Electrochem. Soc. 160 (52013) 77-82.

[42] M. Laleh, F. Kargar, A. Rouhaghdam, Investigations of rare earth sealing of porous micro-arc oxidation coating formed on AZ91D magnesium alloy, J. Rare Earth 30(2012) 1293-1297.

[43] J. Liang, P. Bala Srinivasan, C. Blawert, M. Störmer, W. Dietzel, Electrochemical corrosion behaviour of plasma electrolytic oxidation coatings on AM50 magnesium alloy formed in silicate and phosphate based electrolytes, Electrochim. Acta 54 (2009) 3842-3850.

[44] N. Mora, E. Cano, J.L. Polo, J.M. Puente, J.M. Bastidas, Corrosion protection properties of cerium layers formed on tinplate, Corros. Sci. 46 (2004) 563-578.

[45] M. Dabala, K. Brunelli, E. Napolitani, M. Magrini, Cerium-based chemical conversion coating on AZ63 magnesium alloy, Surf. Coat. Technol. 172 (2003) 227-232.

[46] C. Wang, S. Zhu, F. Jiang, F. Wang, Cerium conversion coatings for AZ91D magnesium alloy in ethanol solution and its corrosion resistance, Corros. Sci. 51 (2009) 2916-2923.

[47] F.H. Scholes, C. Soste, A.E. Hughes, S. G. Hardin, P.R. Curtis, The role of hydrogen peroxide in the deposition of cerium-based conversion coatings, Appl. Surf. Sci. 253 (2006) 1770-1780.

[48] A.E. Hughes, F.H. Scholes, A.M. Glenn, D. Lau, T.H. Muster, S.G. Hardin, Factors influencing the deposition of Ce-based conversion coatings, part I: The role of Al^{3+} ions, Surf. Coat. Technol. 203 (2009) 2927-2936.

[49] A.L. Yerokhin, X. Nie, A. Leyland, A. Matthews, S.J. Dowey, Plasma electrolysis for surface engineering, Surf. Coat. Technol. 122 (1999) 73.

[50] S. Mu, J. Du, H. Jiang, W. Li, Composition analysis and corrosion performance of a Mo–Ce conversion coating on AZ91 magnesium alloy, Surf. Coat. Technol. 2014 DOI: 10.1016/j.surfcoat.2014.06.044.

[51] R.O. Hussein, X. Nie, D.O. Northwood, An investigation of ceramic coating growth mechanisms in plasma electrolytic oxidation (PEO) processing, Electrochim. Acta 112 (2013) 111-119.

[52] B. Hinton, A. Hughes R. Taylor M. Henderson, K. Nelson. L. Wilson, The corrosion protection properties of a cerium oxide conversion coating on aluminium alloy AA2024, ATB Metal J. 37 (1997) 165-168.

[53] E.V. Parfenov, A.L. Yerokhin, A. Matthews, Frequency response studies for the plasma electrolytic oxidation process, Surf. Coat. Technol. 201 (2007) 8661-8670.

[54] A. Fedorockova, P. Raschman, Effects of pH and acid anions on the dissolution kinetics of MgO, Chem. Eng. J. 143(2008) 265-272.

[55] J.A. Mejias, A.J. Berry, K. Refson, D.G. Fraser, The kinetics and mechanism of MgO dissolution, Chem. Phys. Lett. 314 (1999) 558-563.

[56] S.A. Hayes, P. Yu, T.J. O'Keefe, M. J. O'Keefe, J.O. Stoffer, The phase stability of Cerium Species in Aqueous Systems, J. Electrochem. Soc. 149 (2002) 623-630.

[57] D. Chen, L. Wen, W. Gong, G. Wu, J. Wu, Microstructure and formation mechanism of Ce-based chemical conversion coating on 6063 Al alloy, Trans. Nonferrous Met. Soc. China 19 (2009) 592-600.

[58] A.L. Yerokhin, L.O. Snizhko, N.L. Gurevina, A. Leyland, A. Pilkington, A. Matthews, Spatial characteristics of discharge phenomena in plasma electrolytic oxidation of aluminium alloy, Surf. Coat. Technol. 177 (2004) 779-783.

[59] G. Wu, C. Wang, Q. Zhang, P. Kang, Characterization of Ce conversion coating on Gr-f/6061Al composite surface for corrosion protection, J. Alloys Compd. 461 (2008) 389-394.

[60] X. Wang, L. Zhu, X. He, F. Sun, Effect of cerium additive on aluminum-based chemical conversion coating on AZ91D magnesium alloy, Appl. Surf. Sci. 280 (2013) 467-473.

[61] A Conde, J.J de Damborenea, Electrochemical impedance spectroscopy for studying the degradation of enamel coatings, Corros. Sci. 44 (2002) 1555-1567.

[62] S. V. Gnedenkov, S. L. Sinebryukhov, V. I. Sergienko, Electrochemical impedance simulation of a metal oxide heterostructure/electrolyte interface: A review, Russ. J. Electrochem. 42 (2006) 197-211.

[63] R.O. Hussein, D.O. Northwood, X. Nie, The effect of processing parameters and substrate composition on the corrosion resistance of plasma electrolytic oxidation (PEO) coated magnesium alloys, Surf. Coat. Technol. 237 (2013) 357-368.

[64] K. Cho, V. Rao, H. Kwon, Microstructure and electrochemical characterization of trivalent chromium based conversion coating on zinc, Electrochim. Acta 52 (2007) 4449-4456.

[65] J. Sun, G. Wang, Preparation and corrosion resistance of cerium conversion coatings on AZ91D magnesium alloy by a cathodic electrochemical treatment, Surf. Coat. Technol. DOI: 10.1016/j.surfcoat.2014.05.054.

[66] D.Y. Hwang, Y.M. Kim, D.H. Shin, Corrosion resistance of plasma-anodized AZ91 Mg alloy in the electrolyte with/without potassium fluoride, Mater. Trans. 50 (2009) 671-678.

[67] J. Carneiro, J. Tedim, S.C.M. Fernandes, C.S.R. Freire, A.J.D. Silvestre, A. Gandini, M.G.S. Ferreira, M.L. Zheludkevich, Chitosan-based self-healing protective coatings doped with cerium nitrate for corrosion protection of aluminum alloy 2024, Prog. Org. Coat. 75 (2012) 8-13.

[68] H. Shi, E.H. Han, S.V. Lamaka, M.L. Zheludkevich, F. Liu, M.G.S. Ferreira, Cerium cinnamate as an environmentally benign inhibitor pigment for epoxy coatings on AA 2024-T3, Prog. Org. Coat. 77 (2014) 765-773.

[69] J.B. Cambon, J. Esteban, F. Ansart, J.P. Bonino, V. Turq, S.H. Santagneli, C.V. Santilli, S.H. Pulcinelli, Effect of cerium on structure modifications of a hybrid sol–gel coating, its mechanical properties and anti-corrosion behaviour, Mater. Res. Bull. 47 (2012) 3170-3176.

[70] K. Aramaki, Cerium(III) chloride and sodium octylthiopropinate as an effective inhibitor mixture for zinc corrosion in 0.5 M NaCl, Corros. Sci. 44 (2002) 1361-1374.

Figure captions

Figure 1. Optical micrographs of a) PEO, b) PEO_SCe_3g_20min, c) PEO_SCe_10g_20min, d) PEO_SCe_10g_3h.

Figure 2. Backscattered electron images of the coatings plan view a) PEO, b) PEO_SCe_3g_20min, c) PEO_SCe_10g_20min, d) PEO_SCe_10g_3h.

Figure 3. Backscattered electron images of the coatings plan view and respective Ce X-ray elemental maps of: (a,b) PEO_SCe_3g_20min, (c,d) PEO_SCe_10g_20min, (e,f) PEO_SCe_10g_3h.

Figure 4. Backscattered electron images of the cross section of and respective X-ray elemental maps of: (a,b) PEO and Si element, (c,d) PEO_SCe_3g_20min and Ce element, (e,f) PEO_SCe_10g_20min and Ce element, (g,h) PEO_SCe_10g_3h and Ce element.

Figure 5. X-ray diffraction patterns of unsealed and sealed PEO coatings.

Figure 6. Impedance spectra of PEO coated sample up to three days of immersion in 0.5wt.% NaCl solution: (a, b) Bode plots and (c) Nyquist plot

Figure 7. Impedance spectra of PEO_SCe_3g_20min coated sample up to three days of immersion in 0.5wt.% NaCl solution: (a, b) Bode plots and (c) Nyquist plot.

Figure 8. Impedance spectra of PEO_SCe_10g_20min coated sample up to three days of immersion in 0.5 wt.% NaCl solution: (a, b) Bode plots and (c) Nyquist plot

Figure 9. Impedance spectra of PEO_SCe_10g_3h coated sample up to three days of immersion in 0.5 wt.% NaCl solution: (a, b) Bode plots and (c) Nyquist plot.

Figure 10. Equivalent circuit used for simulation of the electrical parameters inserted in an example of the fitting of the experimental data.

Figure 11. Values of the total resistance (out+in+polar) for all the materials up to 3 days of immersion in 0.5 wt. % NaCl solution.

Figure 12. Evolution of resistance for all the materials with the immersion time up to 3 days of immersion in 0.5 wt. % NaCl solution a) R_{polar} b) R_{in}

Figure 13. Backscattered electron image of the cross section of PEO_SCe_10g_3h after 3 days of immersion in 0.5 wt.% NaCl solution.

Table 1. Sealing post-treatment methods.

Material	Solution	Temperature (°C)	Time (min)
PEO_SCe_3g_20min	3 g/l $Ce(NO_3)_3$, 0.3 g/l H_2O_2 and 1 g/l H_3BO_3	30	20
PEO_SCe_10g_20min	10 g/l $Ce(NO_3)_3$, 0.3 g/l H_2O_2 and 1 g/l H_3BO_3	30	20
PEO_SCe_10g_3h	10 g/l $Ce(NO_3)_3$, 0.3 g/l H_2O_2 and 1 g/l H_3BO_3	30	180

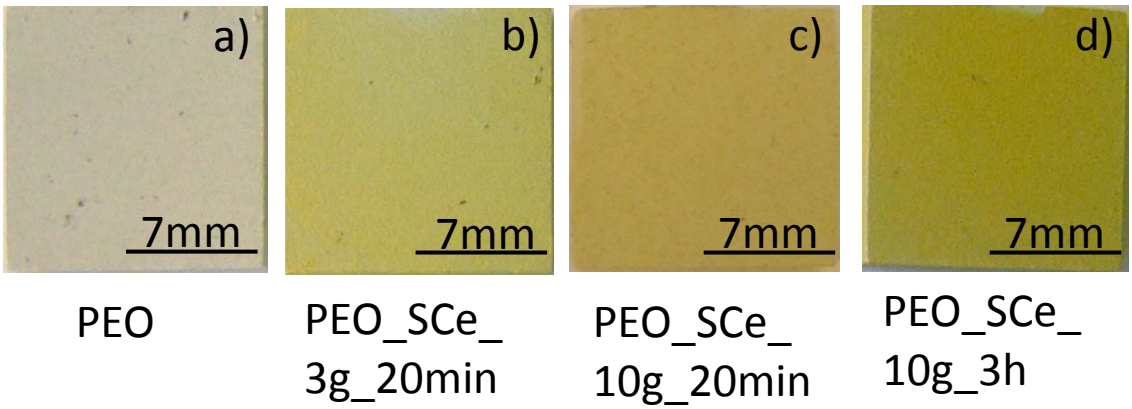
a)
7mm
b)
7mm
c)
7mm
d)
7mm
PEO
PEO_SCe_
3g_20min
PEO_SCe_
10g_20min
PEO_SCe_
10g_3h

Figure 1.

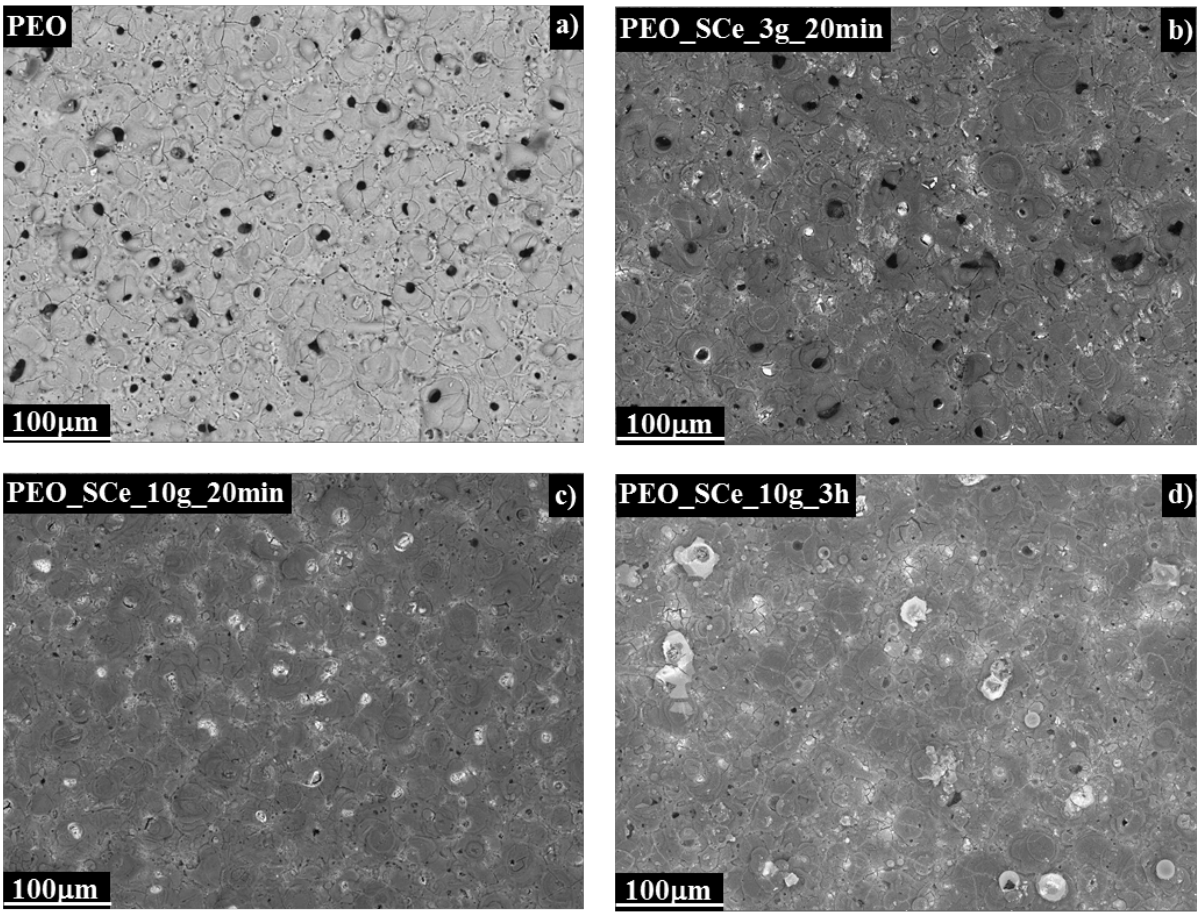
PEO
a)
100µm
PEO_SCe_3g_20min
b)
100µm
PEO_SCe_10g_20min
c)
100µm
PEO_SCe_10g_3h
d)
100µm

Figure 2.

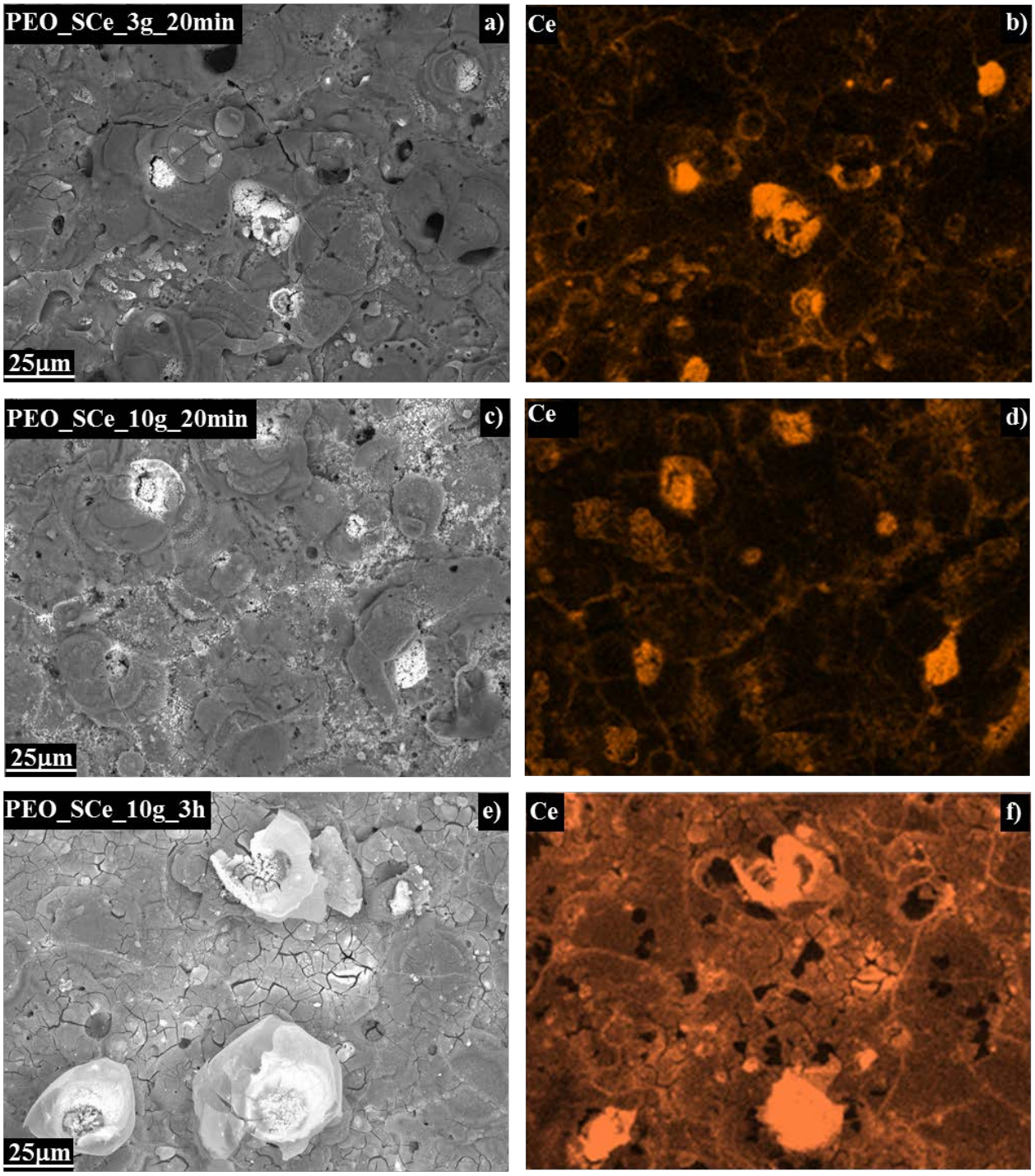
PEO_SCe_3g_20min
a)
25µm
Ce
b)
PEO_SCe_10g_20min
c)
25µm
Ce
d)
PEO_SCe_10g_3h
e)
25µm
Ce
f)

Figure 3.

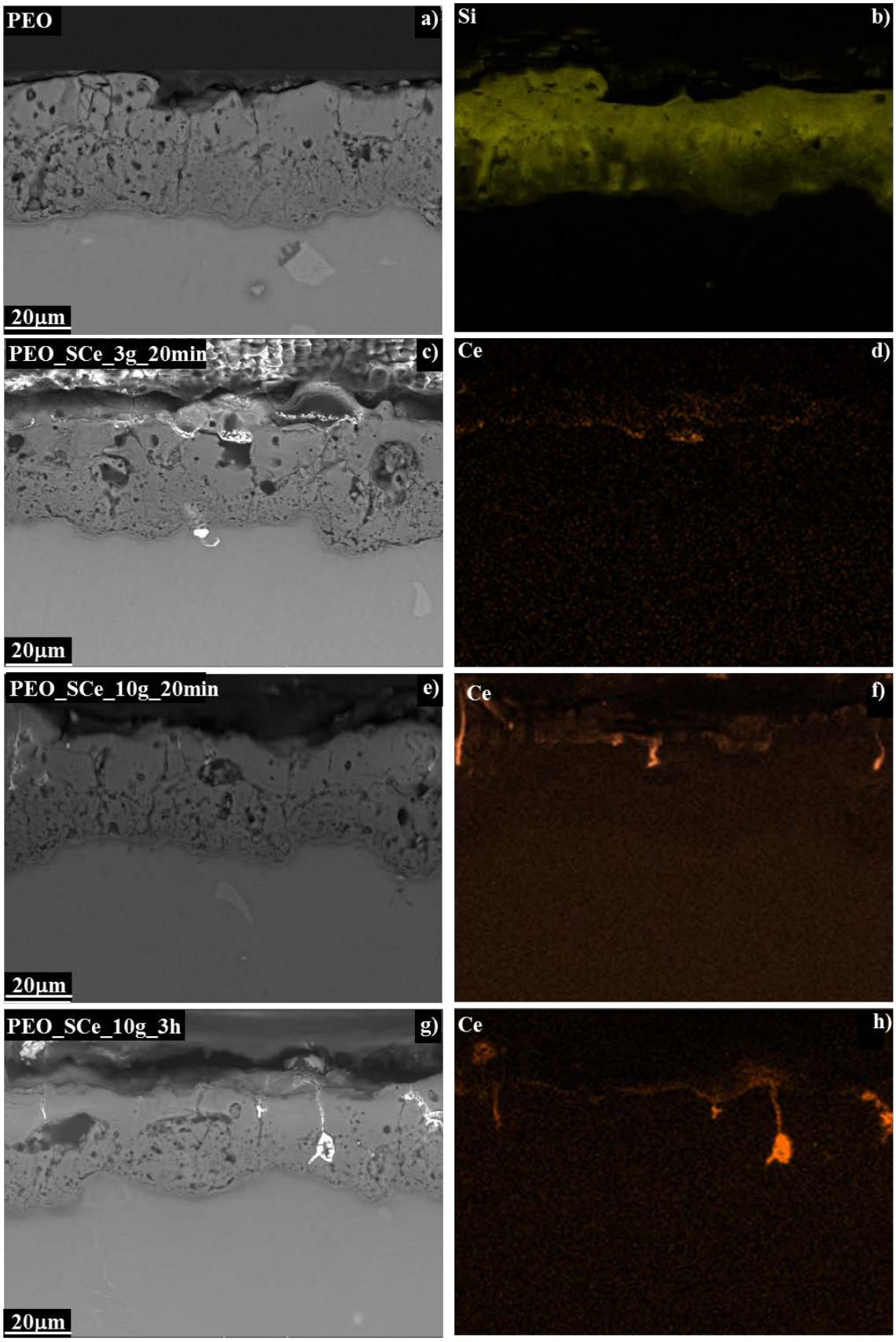
PEO
a)
20µm
Si
b)
PEO_SCe_3g_20min
c)
20µm
Ce
d)
PEO_SCe_10g_20min
e)
20µm
Ce
f)
PEO_SCe_10g_3h
g)
20µm
Ce
h)

Figure 4.

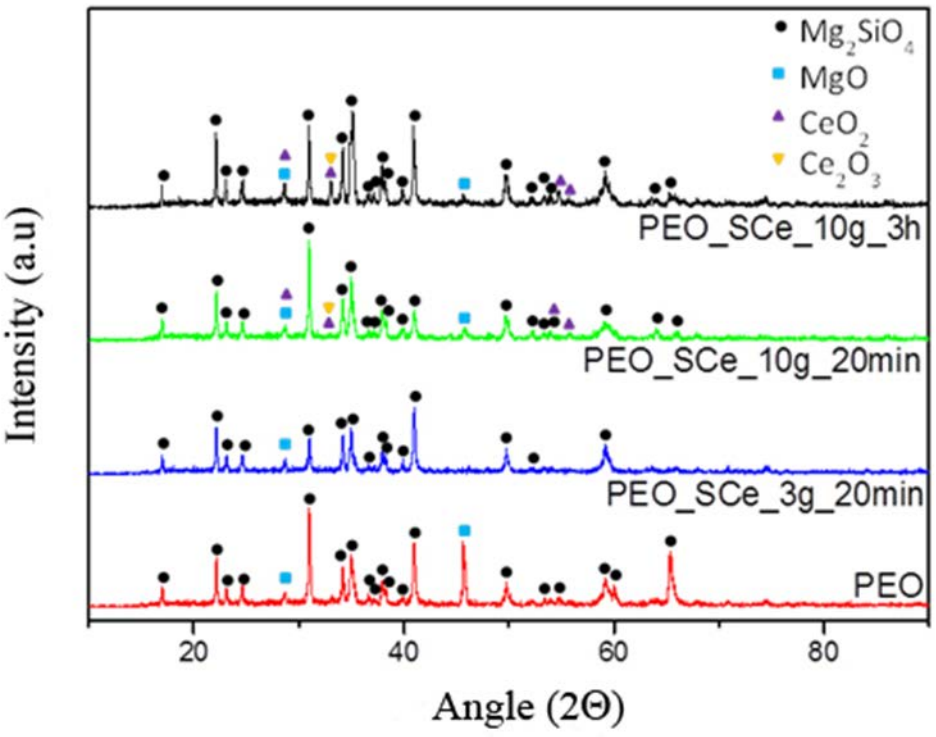
Mg2SiO4
MgO
CeO2
Ce2O3
PEO_SCe_10g_3h
PEO_SCe_10g_20min
PEO_SCe_3g_20min
PEO
Intensity (a.u)
20
40
60
80
Angle (2Θ)

Figure 5.

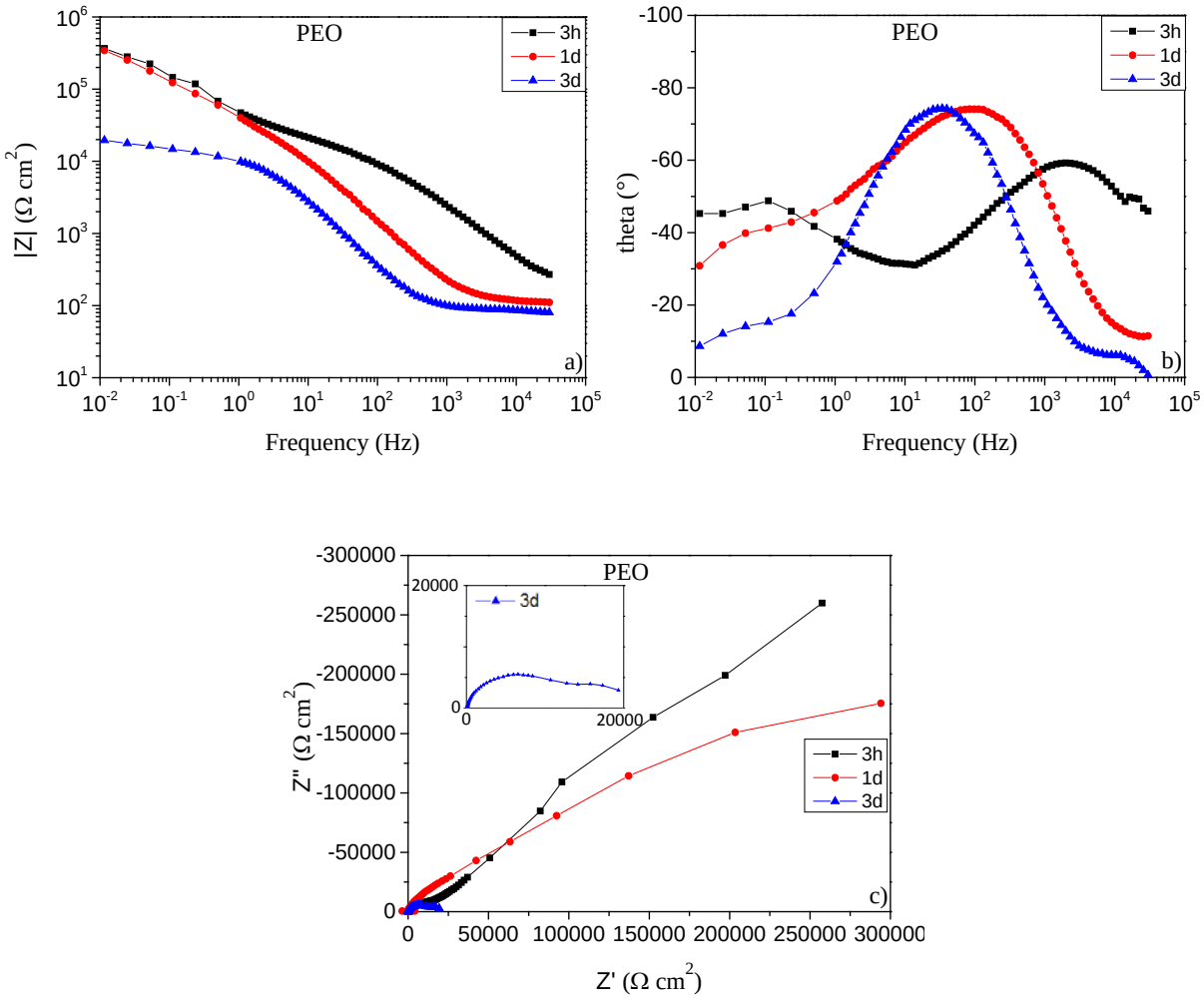

Figure 6.

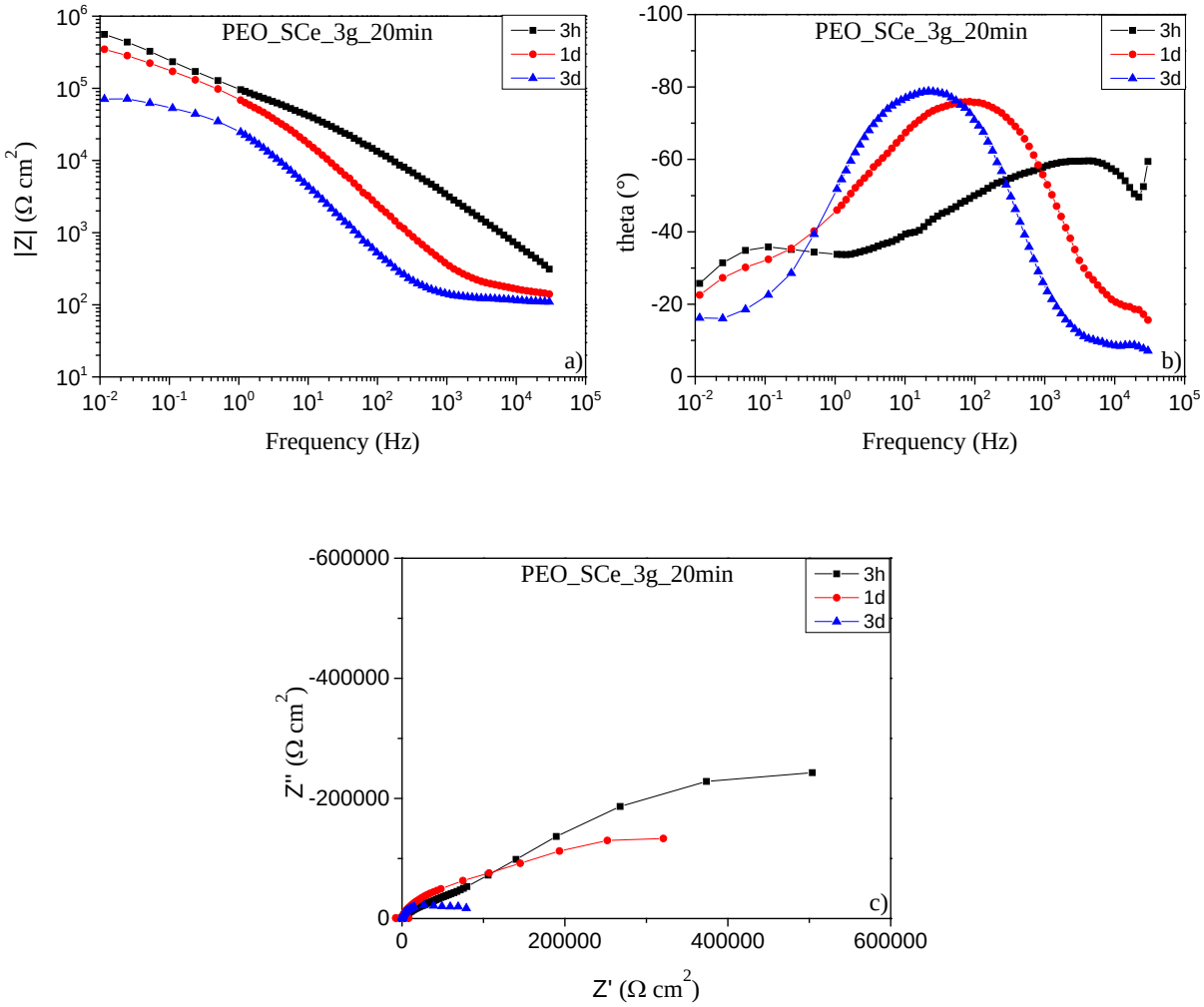
PEO_SCe_3g_20min
3h
1d
3d
|Z| (Ω cm2)
Frequency (Hz)
a)
theta (°)
b)
Z'' (Ω cm2)
Z' (Ω cm2)
c)

Figure 7.

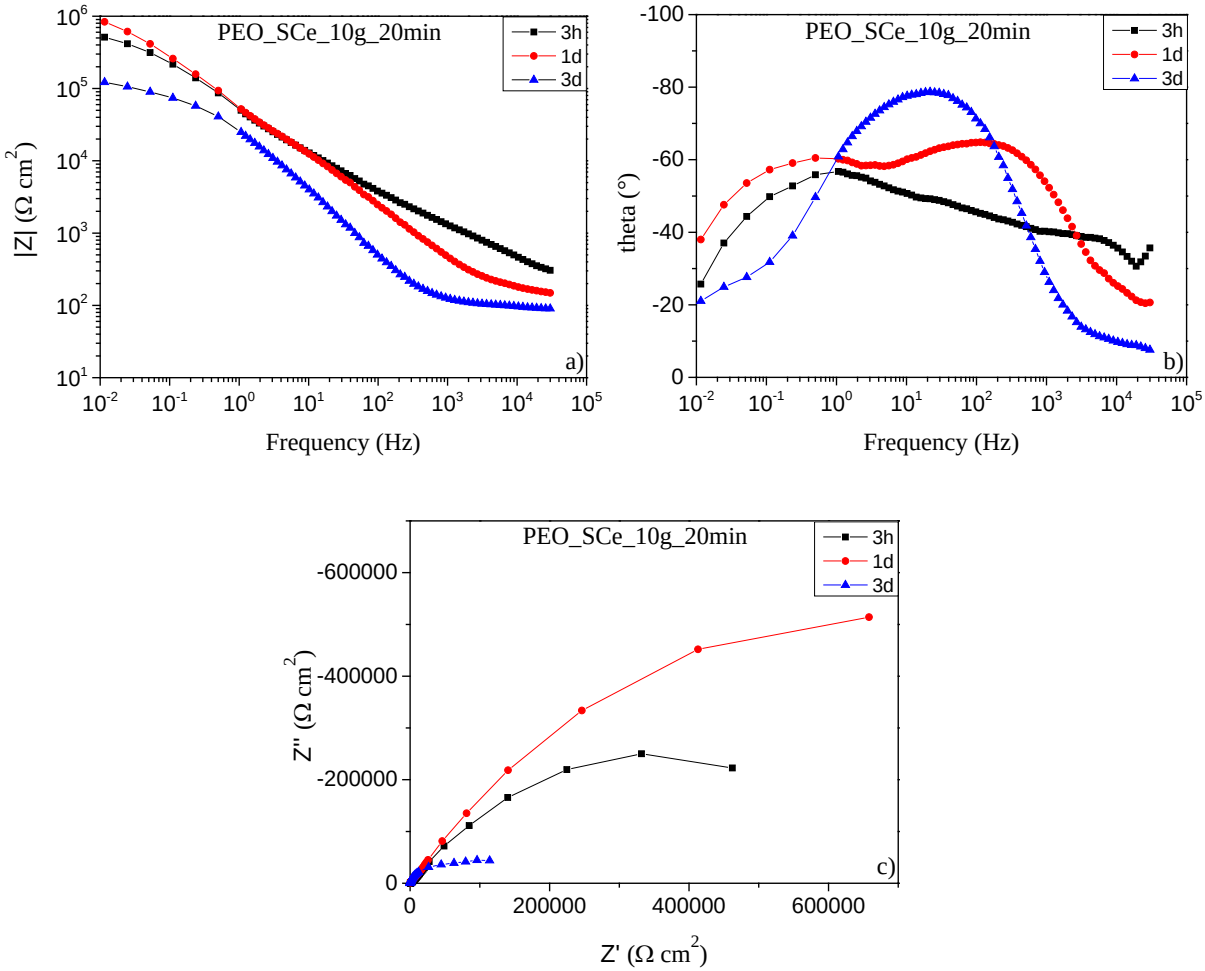
PEO_SCe_10g_20min
3h
1d
3d
|Z| (Ω cm2)
Frequency (Hz)
a)
theta (°)
b)
Z'' (Ω cm2)
Z' (Ω cm2)
c)

Figure 8.

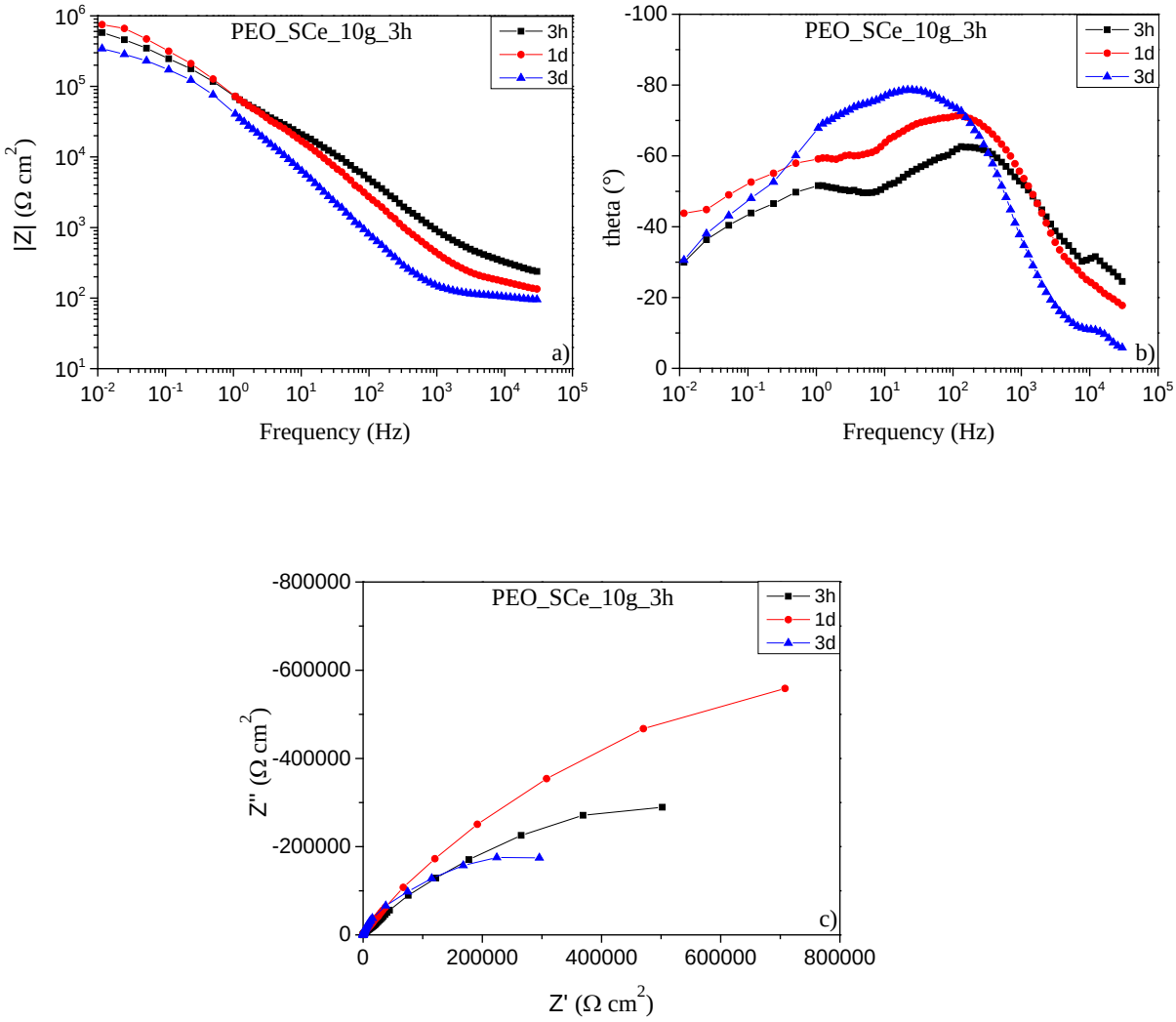
PEO_SCe_10g_3h
3h
1d
3d
|Z| (Ω cm2)
Frequency (Hz)
a)
theta (°)
b)
Z'' (Ω cm2)
Z' (Ω cm2)
c)

Figure 9.

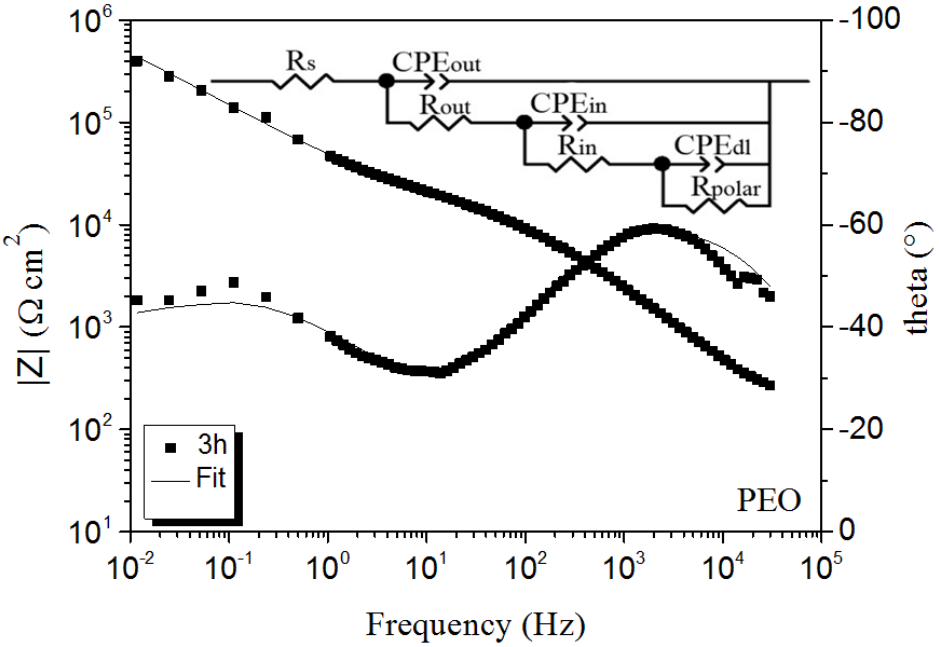
Rs
CPEout
Rout
CPEin
Rin
CPEdl
Rpolar
3h
Fit
PEO
|Z| (Ω cm2)
theta (°)
Frequency (Hz)

Figure. 10

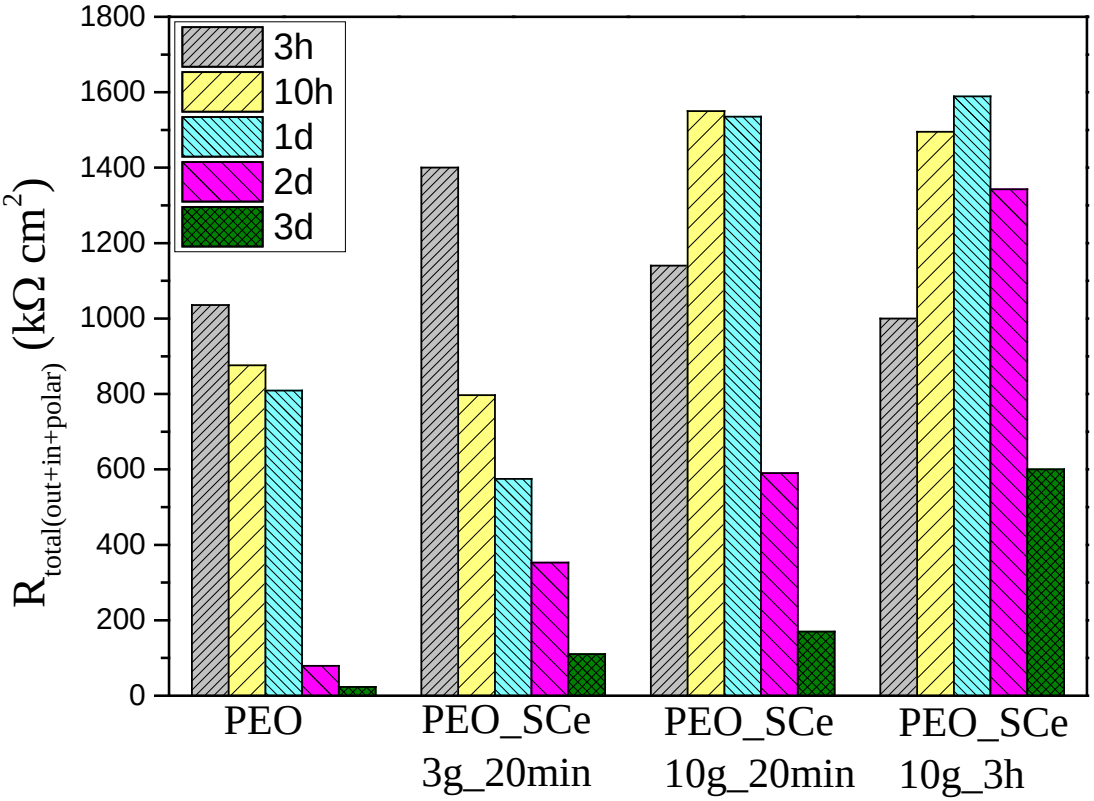
1800
1600
1400
1200
1000
800
600
400
200
0
3h
10h
1d
2d
3d
$R_{total(out+in+polar)}$ (kΩ cm^2)
PEO
PEO_SCe 3g_20min
PEO_SCe 10g_20min
PEO_SCe 10g_3h

Figure 11.

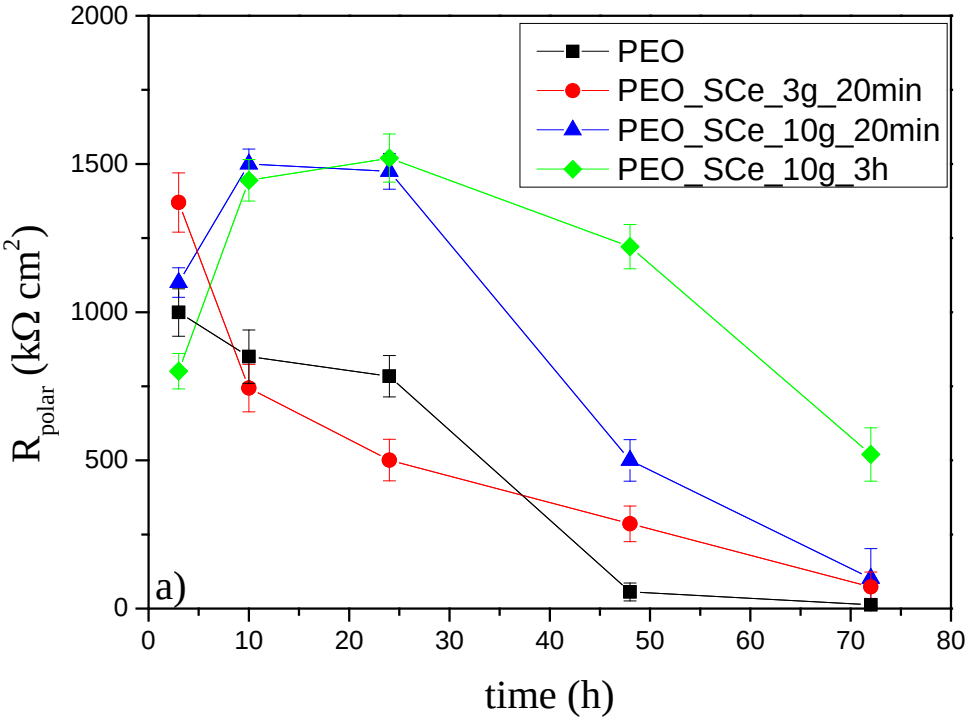
PEO
PEO_SCe_3g_20min
PEO_SCe_10g_20min
PEO_SCe_10g_3h
a)
R_{polar} (kΩ cm^2)
time (h)
0
500
1000
1500
2000
0
10
20
30
40
50
60
70
80

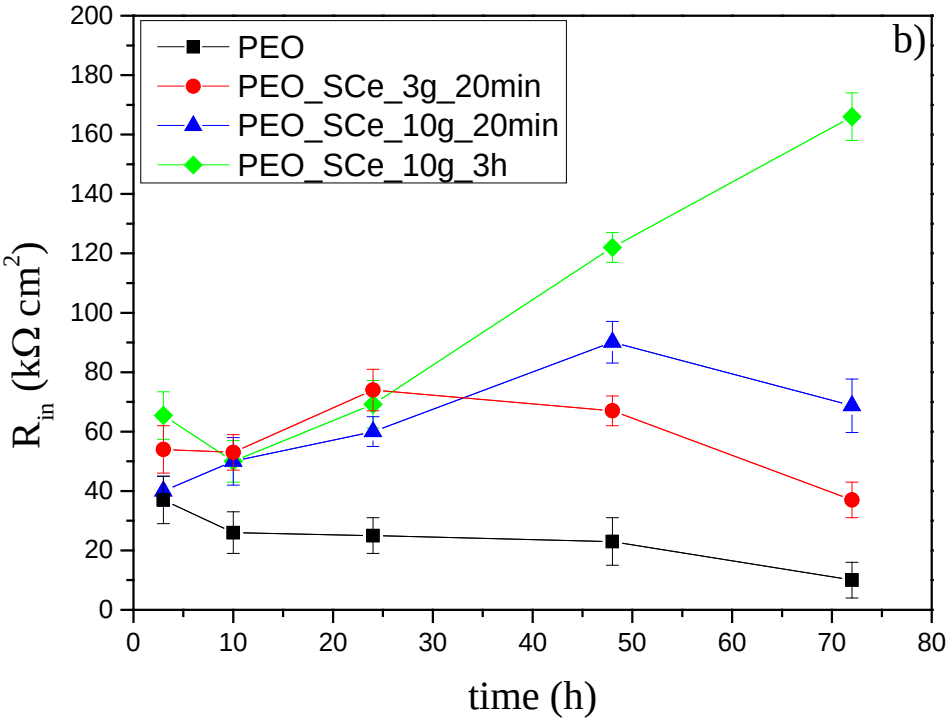
PEO
PEO_SCe_3g_20min
PEO_SCe_10g_20min
PEO_SCe_10g_3h
b)
R_{in} (kΩ cm^2)
time (h)
0
20
40
60
80
100
120
140
160
180
200
0
10
20
30
40
50
60
70
80

Figure 12.

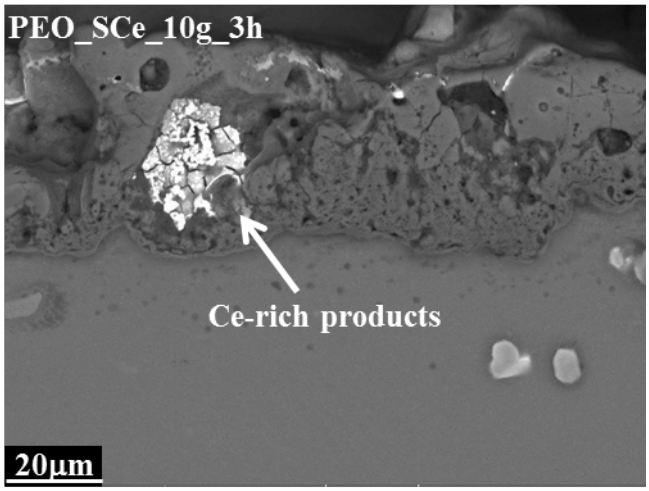

Figure 13.